International Journal of Minerals, Metallurgy and Materials
Volume 26, Number 7, July 2019, Page 901
https://doi.org/10.1007/s12613-019-1817-6

Effects of Ta on the solidification behavior and microstructure of a rhenium-containing hot corrosion resistant single crystal

Shi-hua Ma[1,2], *Hong-quan Hao*[3], *Dong Wang*[1], *Lang-hong Lou*[1], *and Jian Zhang*[1]

1) Institute of Metal Research, Chinese Academy of Sciences, Shenyang 110016, China
2) School of Materials Science and Engineering, University of Science and Technology of China, Shenyang 110016, China
3) National Natural Science Foundation of China, Beijing 100085, China
(Received: 29 October 2018; revised: 24 December 2018; accepted: 27 December 2018)

Abstract: The effects of Ta on the solidification microstructure of the Re-containing hot corrosion resistant Ni-base single crystal were investigated. Results showed that Ta addition significantly modified the solidification behavior and further influenced the as-cast microstructure. Ta addition changed the solidification characteristic temperatures and decreased the segregation of refractory elements (Re and W) as well as increased the solidification temperature range from 39.0 to 61.8°C as Ta addition increased from 2wt% to 8wt%. The integration of these two factors increased the primary dendrite arm spacing and changed the morphology and size of γ′ precipitates. With increasing Ta addition from 2wt% to 8wt%, the size of γ′ precipitates in the dendrite core increased substantially from 0.24 to 0.40 μm, whereas the γ′ precipitates in the interdendritic region decreased slightly from 0.56 to 0.47 μm. This paper then discussed the mechanism of these "Ta effects".

Keywords: superalloys; tantalum; solidification behavior; microstructure

1. Introduction

Hot corrosion resistant single crystal (SX) superalloys are critical engineering materials of hot-section components in industrial gas turbines (IGTs) that operate in hot corrosion environment and under complex loading at high temperature for long time. As the inlet temperature of IGTs continues to rise, the high-temperature capabilities of hot corrosion resistant single-crystal turbine blades should be improved [1–2]. As per the development experience of superalloys for aero-engines, optimizing the composition of alloys by adding refractory elements (Re, W, Mo, and Ta) would be useful and effective to improve the high-temperature strength of alloys for IGTs [3–5]. However, considering the harsh hot corrosive in-service environment where IGT blades operate, scholars must explore a feasible refractory element that may not only improve the high-temperature strength but also improve or not deteriorate at least the hot corrosion resistance of the alloy.

Among refractory elements, W and Mo exhibit a detrimental effect on hot corrosion resistance by inducing acidic fluxing and accelerating corrosion [2,6]. Re and Ta significantly improve the high-temperature strength and hot corrosion resistance of alloy [6–9] and may be the best choice for hot corrosion alloys to obtain higher temperature capabilities. Given the large size of IGT blades, adding Re is difficult to implement under commercial condition. Furthermore, microstructure stability may be damaged upon Re addition during service because it facilitates the formation of Re-rich topologically close-packed (TCP) phases, especially in high-Cr hot corrosion resistant superalloys [10]. Consequently, a feasible alloying approach, i.e., adding Ta to low-Re or Re-free alloy, may effectively improve the high-temperature capabilities of hot corrosion resistant Ni-based superalloys.

Any composition design approach must make use of suitable composition–microstructure–property relationships. An in-depth understanding of how adding Ta influences solidification behavior and as-cast microstructure is important and critical to the development of hot corrosion resistant

Corresponding author: Wang Dong E-mail: dwang@imr.ac.cn

Ni-based superalloys with high Cr content. As a strong γ′-forming element, Ta can significantly modify the solidification characteristics of Ni-based superalloys [11]. With increasing Ta content, the γ′ volume fraction increases [9,12–13]. Furthermore, adding Ta tends to lower the γ/γ′ lattice misfit and leads to an evolution in the morphology of γ′ precipitates [14–15]. Nevertheless, apart from these well-known "Ta-effects," controversies remain regarding the role of Ta in solidification characteristics, particularly in dendrite arm spacing and γ′ precipitates size, because Ta appears to enlarge or reduce the freezing temperature range depending on the specific SX superalloys. Gao *et al*. [16–17] reported that the as-cast dendrite arm spacing was approximately equal among all Ta-doped IN716 alloys given the lack of obvious change in solidification characteristic temperatures and freezing temperature. By contrast, Han [18] revealed that with increasing Ta content, the primary and secondary dendrite spacing increased in the as-cast directionally solidified Ni-based superalloy; nevertheless, the specific mechanism was unclear. In general, Ta addition inhibited the coagulation of γ′ phase and helped refine the γ′ phase [9,19]. However, several experimental results indicated that with increasing Ta content, the size of γ′ in dendrite increased; meanwhile, the size of γ′ in the interdendritic region had variable sizes and morphologies, with some γ′ apparently larger or smaller than the others. Thus far, the mechanism of how Ta affects the γ′ phase remains unknown [18,20].

Few studies have focused on the effects of Ta addition on solidification behavior and microstructure, particularly in high Cr and Re-containing hot corrosion resistant Ni-based SX superalloys; in this regard, a systematic study of "Ta effects" should be conducted. In the present paper, the effect of Ta addition on the solidification behavior and microstructure of a hot corrosion resistant 2Re10Cr model Ni-based SX superalloy was systematically investigated. Results, including solidification characteristic temperatures, as-cast microstructure analysis, and constituent element segregation, can be helpful for understanding and elucidating the mechanism of how Ta addition affects solidification microstructure. This work provides theoretical basis for developing hot corrosion resistant alloys.

2. Experimental

2.1. Materials and specimen preparation

Three alloys doped with 2.0wt%, 5.0wt%, and 8.0wt% Ta were designed to study the influence of Ta on the solidification behavior and microstructure of Re-containing hot corrosion Ni-based SX superalloys. The compositions of the alloys are shown in the Table 1. Each alloy was named after its concentrations of Ta, i.e., 2Ta, 5Ta, and 8Ta. SX rods were fabricated using high-rate solidification (HRS) method at a withdrawal rate of 3 mm/min. All SX rods of experimental alloys were measured in diameter of 16 mm and in the length of 220 mm.

Table 1. Nominal compositions of experimental alloys wt%

Alloys	Al+Ti	Cr	Co	Mo	W	C	Re	Ta	Ni
2Ta	7.5	9.5	8	0.5	4.5	0.04	2	2	Bal.
5Ta	7.5	9.5	8	0.5	4.5	0.04	2	5	Bal.
8Ta	7.5	9.5	8	0.5	4.5	0.04	2	8	Bal.

All of the as-cast specimens were sectioned at approximately 10 mm above the starter block to ensure the consistency and accuracy of the results. Samples were prepared using the standard metallographic procedures of grinding followed by mechanically polishing. Only the specimens for microstructure analysis were electrochemically etched (etching solution: 30 mL of HCl, 10 mL of HNO_3, 40 mL of C_3H_7OH; applied voltage: 10 V; time: 10 s), and the other specimens were in the as-polished state.

2.2. Differential thermal analysis

The effects of Ta addition on solidification characteristic temperatures were investigated using differential scanning calorimetry (DSC, NETZSCH 404C). DSC experiments were performed in high-purity alumina crucibles, which were heated first from 1100 to 1450°C at 10°C/min under the protection of argon atmosphere and then cooled to 1100°C at the same rate. Solidification characteristic temperatures were determined by plotting the DSC signal ($W \cdot mg^{-1}$) against temperature (°C). Despite that the transition temperatures characterized by the cooling curves decrease because of supercooling [21], the precipitate temperature of γ′ and eutectic temperature is more sensitive and easier to character in the cooling curves. Hence, the derivatives of the DSC heating and cooling curves were chosen to characterize the solidus and liquidus temperatures in the heating curves and reveal the influence of Ta content on characteristic temperatures. The temperature at the maximum of γ′ precipitation reactions, T_γ, was determined by the small exothermic peak in the cooling curves.

2.3. Microstructure analysis and characterization

Microstructural analysis of the as-cast specimens was conducted using optical microscope (OM, Zeiss Axiovert 200 MAT) and field-emission scanning electron microscope (SEM, Zeiss Supra 35). At least five OM fields for each

sample were chosen to characterize the average primary dendrite arm spacing (PDAS, λ_1) of the solidification microstructure, which can be expressed as

$$\lambda_1 = 1/\sqrt{N} \quad (1)$$

where N is the number of dendrites per unit (μm^2) [22]. Considering the irregular γ′ morphology of the as-cast samples, the shape of individual γ′ was regarded as spherical to ensure consistency [23]. The average sizes of γ′ precipitates (d) were determined by calculating the mean diameter of more than 200 γ′ precipitates. The volume fraction of γ′ and eutectic phases (f) were determined using an American National Standard: Standard Test Methods for Determining Volume Fraction by Systematic Manual Point Count (No. ASTM E562-2011). The detailed measurement process is as follows. The SEM photos for γ′ precipitates were first processed in Adobe Photoshop CS6 to draw grids with size approximately twice as large as that of the γphase. The percentage of the points on the phases of interest, i.e., γ′ or eutectic phases, was determined as volume fraction.

2.4. Electron microprobe analysis

The element segregation of the as-cast alloys was characterized using electron microprobe analysis (EPMA, JEOL JXA-8230) with wavelength dispersive spectrometers (WDS, acceleration voltage: 20 kV; beam current:10 nA) to investigate the effect of Ta addition on solidification behavior. The segregation behavior of the constituent elements in the experimental alloys was characterized. Five different positions in each alloy were chosen to quantitatively determine mean dendritic (C_d) and interdendritic composition (C_{id}). The segregation ratio (k) of individual elements was then calculated as follows:

$$k = C_d / C_{id} \quad (2)$$

3. Results

3.1. Differential scanning calorimetry analysis

The comparisons between the heating and cooling curves of 5Ta2Re alloy are shown in Fig. 1(a). The specific liquidus temperature (T_L) and the solidus temperature (T_S) in the cooling curves decreased by approximately 15°C and 25°C, respectively, compared with those in the heating curves due to supercooling. Fig. 1(b) shows that the γ′ phase peak precipitation temperature ($T_{\gamma'}$) increased substantially with increasing Ta content, thereby indicating improved stability of γ′ phases. By contrast, the liquidus and solidus temperatures decreased with increasing Ta content, as shown in Fig. 1(c). Furthermore, compared with the liquidus temperature (T_L),

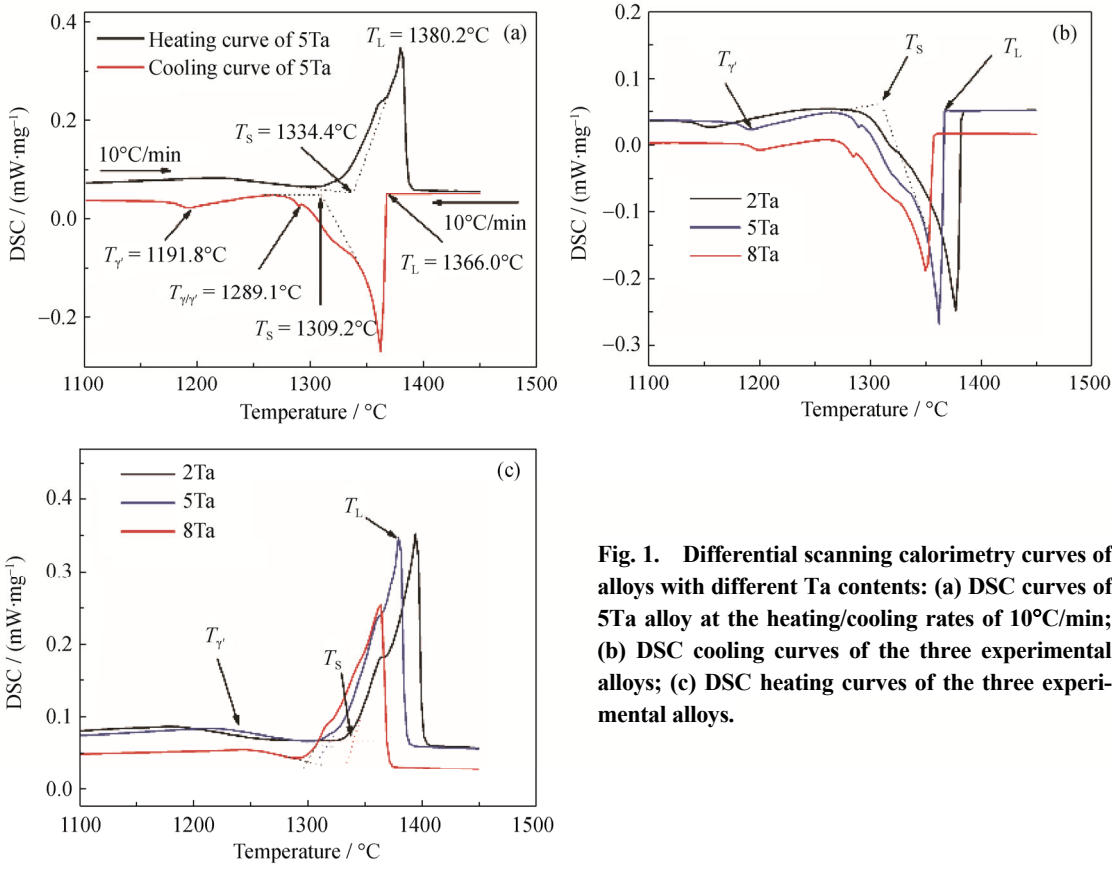

Fig. 1. Differential scanning calorimetry curves of alloys with different Ta contents: (a) DSC curves of 5Ta alloy at the heating/cooling rates of 10°C/min; (b) DSC cooling curves of the three experimental alloys; (c) DSC heating curves of the three experimental alloys.

the solidus temperature (T_S) decreased more seriously and resulted in a larger solidification temperature range ($\Delta T = T_L - T_S$) in alloys with increasing Ta content. The specific values are listed in Table 2. The solidification temperature range increased from 39.0°C (2Ta) to 45.8°C (5Ta) and then finally increased to 61.8°C (8Ta).

3.2. Effect of Ta on the as-cast microstructure

Fig. 2 depicts the typical transverse sections showing the "crossing" dendrite morphology of the as-cast microstructure in the experimental alloys. The volume fraction of γ/γ′ eutectic phases (white area in Fig. 2) increased remarkably with Ta content. Additionally, the PDAS of the alloys increased by approximately 20 and 40 μm, respectively, when the Ta content was increased by per 3wt% within a range of 2wt%–8wt% (Table 3). Hence, this effect was more obvious in alloys containing high levels of Ta.

Fig. 3 shows the typical SEM micrographs of the three as-cast experimental alloys. Every four γ′ phases were tied up and exhibited a flower-like morphology. With increasing Ta content, the morphology of the individual γ′ phase gradually evolved from the initial near-spherical shape to cuboidal shape and the volume fraction of γ′ precipitates

Table 2. Solidification characteristic temperatures of alloys measured by DSC °C

Alloys	T_S	T_L	T_γ	ΔT
2Ta	1356.2	1395.2	1156.9	39.0
5Ta	1334.4	1380.2	1191.8	45.8
8Ta	1301.8	1363.6	1195.7	61.8

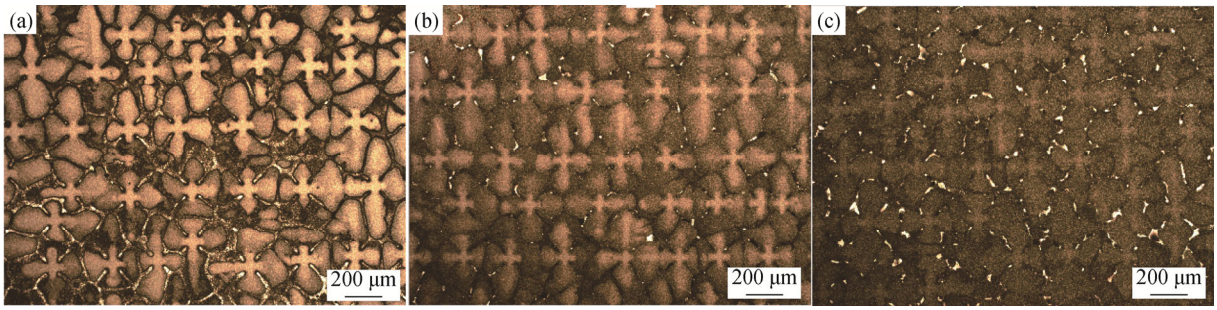

Fig. 2. Optical images of the as-cast microstructures on the transverse section in the three alloys: (a) 2Ta, (b) 5Ta, and (c) 8Ta.

Table 3. Microstructure characteristics of as-cast alloys with different Ta contents

Alloys	λ_1 / μm	γ′ in dendritic core		γ′ in interdendritic region	
		d / μm	f / %	d / μm	f / %
2Ta	307.47 (±7.77)	0.241	42.74 (±2.03)	0.558	51.08 (±1.33)
5Ta	334.46 (±10.03)	0.316	49.40 (±1.96)	0.505	54.36 (±2.87)
8Ta	374.18 (±11.81)	0.397	54.78 (±2.47)	0.474	61.76 (±1.57)

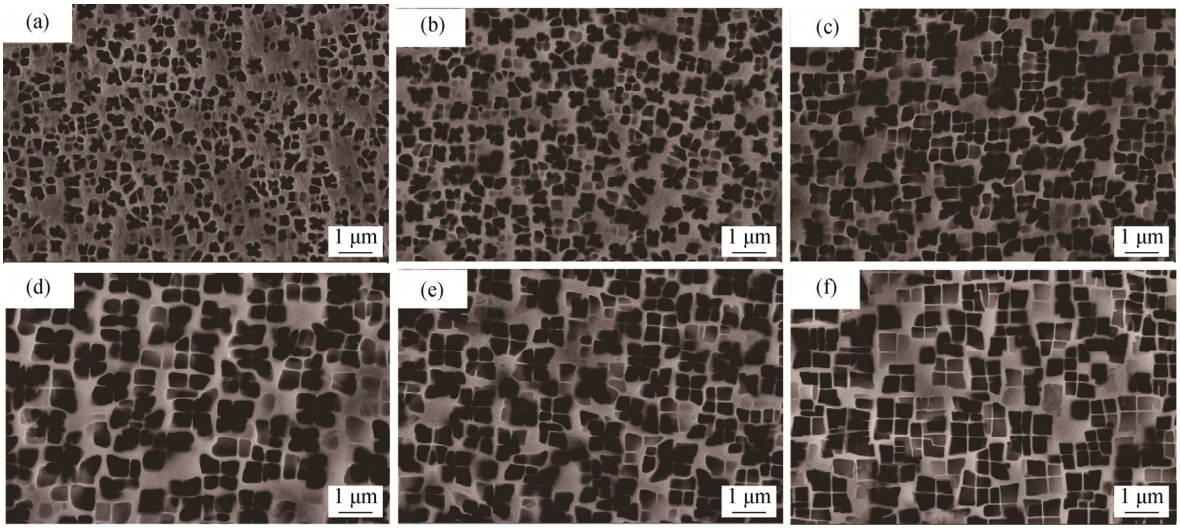

Fig. 3. γ' morphology of (a) 2Ta, (b) 5Ta and (c) 8Ta as-cast alloys in the dendrite core, and of (d) 2Ta, (e) 5Ta and (f) 8Ta as-cast alloys in the interdendritic region.

increased. The size of γ′ precipitates in the interdendritic region was larger than that in the dendrite cores. Ta addition exhibited opposite effects on the size change of the γ′ precipitates in different regions. With increasing Ta content, the size of γ′ precipitates in the dendrite core increased substantially, whereas that of γ′ precipitates in the interdendritic region slightly decreased, leading to an increase in the homogeneity of γ′ precipitations in the whole dendrite structure.

3.3. Solidification segregation characteristics

Fig. 4 shows the segregation ratios (k) of alloying elements in the three alloy samples between the dendrite core and the interdendritic region in relation to the segregation degree during solidification. The values of segregation ratios (k), ones that are closer to 1, indicate a less pronounced segregation degree of these constituents during solidification. As shown in the Fig. 4, W and Re were strongly segregated to the dendrite cores in the three alloys, whereas Ta, Ti, and Al were obviously segregated to the interdendritic region. Further comparison in the k of the constituent alloying elements in alloys with different Ta contents, the k values of W, Re, Ti, and Ta were all closer to unity and then revealed the segregation of them gradually weakened upon Ta addition. The detailed measured values are listed in Table 4. The segregation ratios (k) of W and Re decreased from 3.04 (2Ta) to 1.55 (8Ta) and from 3.98 (2Ta) to 1.77 (8Ta), respectively.

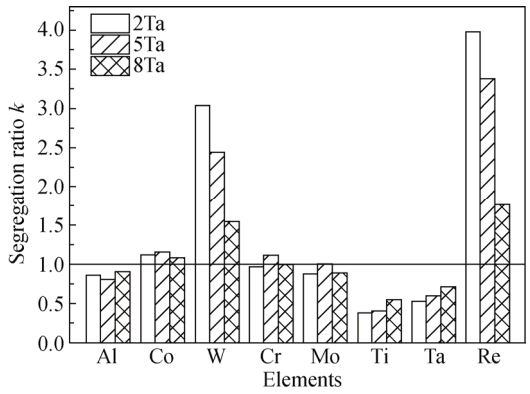

Fig. 4. Segregation ratio k of alloying elements in the three as-cast alloys between the dendrite core and the interdendritic region.

Table 4. Compositions of different regions in the three as-cast alloys measured by EPMA

Alloys	Regions	Al	Co	W	Cr	Mo	Ti	Ta	Re	Ni
2Ta	Dendrite core (C_d / wt%)	4.08	8.59	5.50	9.53	0.41	1.56	1.23	3.43	65.09
	Interdendritic (C_{id} / wt%)	4.73	7.6	1.81	9.79	0.47	4.04	2.32	0.86	67.99
	k (C_d/C_{id})	0.86	1.13	3.04	0.97	0.87	0.39	0.53	3.99	0.96
5Ta	Dendrite core (C_d / wt%)	4.10	8.59	5.48	9.38	0.45	1.73	3.23	3.46	63.17
	Interdendritic (C_{id} / wt%)	5.08	7.39	2.25	8.41	0.44	4.27	5.39	1.02	65.53
	k (C_d/C_{id})	0.81	1.16	2.44	1.12	1.02	0.40	0.60	3.39	0.96
8Ta	Dendrite core (C_d / wt%)	4.41	8.35	4.76	9.72	0.42	1.71	5.53	3.04	60.61
	Interdendritic (C_{id} / wt%)	4.89	7.66	3.07	9.82	0.47	3.13	7.79	1.71	60.57
	k (C_d/C_{id})	0.90	1.09	1.55	0.99	0.89	0.55	0.71	1.78	1.00

4. Discussion

The experimental results provide clear evidence that Ta content significantly affects the solidification behavior and microstructure of Re-containing hot corrosion resistant Ni-based superalloys. The effect of Ta content on (i) PDAS and (ii) the size and shape evolution of γ′ precipitates was also determined. According to the Hunt model [24], PDAS (λ_1) can be expressed as Eq. (3).

$$\lambda_1 = \frac{2.83\left(k_0 \Delta T D \Gamma\right)^{1/4}}{V^{1/4} G^{1/2}} \tag{3}$$

where k_0 is the equilibrium distribution coefficient, D is the diffusion coefficient in the liquid, Γ is the Gibbs–Thomson coefficient, V is the growth velocity, G is the temperature gradient, and ΔT is the solidification temperature range. In the present investigation, the PDAS (λ_1) increased with solidification temperature range. The decrease in the solidus temperature was sharper than that in the liquidus temperature, and the solidification temperature range increased with Ta addition, especially in high Ta-containing alloys, consistent with the Ni–Ta binary phase diagram. Consequently, the primary dendrite spacing increased with Ta content. These experimental results are similar to those reported by Gao *et al.* [16] on IN716 alloys added with 0wt%–2.0wt% Ta, indicating the Hunt model can well unveil the relationship between Ta content and PDAS.

The growth of γ′ precipitates is mainly concerned with T_{γ} and refractory element distribution. During solidification, a

sufficient number of γ′ precipitates nucleated at the peak T_γ and then started to grow when reaching the critical interparticle distance [25]. A higher peak T_γ means a longer time for γ′ precipitates to grow sufficiently and thus possess a larger size. Ta addition slightly lowers the extent of refractory element segregation (Re and W) and further affects the element partition to the dendritic cores and interdendritic region. Given that Re and W may substantially decrease the γ′ precipitate growth kinetics [12,26], the change in element segregation causes different diffusion rates in the dendritic core and interdendritic region and leads to differences in the size of γ′ precipitates.

With respect to the γ′ precipitates in the dendritic cores, T_γ was improved with increasing Ta content. Moreover, Ta addition was more effective in suppressing refractory element segregation in the dendritic cores of alloys containing high Ta content. Therefore, the combination of higher T_γ and less refractory element concentration reduced diffusion inhibition and promoted the growth of γ′ precipitates in dendritic cores. For γ′ precipitates in the interdendritic region, with Ta addition, more refractory elements (Re and W) partitioned to the interdendritic region and inhibited the growth controlled by diffusion, although T_γ was found to be higher. This phenomenon caused the decrease in the size of γ′ precipitates and the increase in the volume fraction with Ta addition.

Extensive investigations on Ni-based alloys demonstrated that γ′ precipitate shapes are substantially influenced by variations in lattice misfit due to the changes in the overall compositions and partitioning of elements to the precipitates and matrix phases [14,27–28]. A crystal lattice parameter is related to composition and thus depends on the atomic radius. Ta solute has larger atomic size than Ni by approximately 15%–18%. The increased lattice parameter of fcc γ-Ni is larger than that of γ′-Ni_3Al. In general, alloys with more negative lattice misfit possess more cuboidal γ′ precipitates [29]. Thus, Ta addition caused a decrease in lattice misfit and the evolution of γ′ precipitate shapes.

This study also indicated the less segregation of refractory elements (especially for Re and W) upon Ta addition. In contrast to Re and W, Ta was mainly segregated to the interdendritic region. During the solidification, the content of Ta distributed in the dendritic cores increased with increasing level of Ta added. High amounts of Ta added may exclude Re and W from the dendritic cores to the interdendritic region, resulting in less segregation of those elements. In summary, Ta addition can effectively modify the segregation and microstructure characteristics and improve homogeneity of both alloys.

5. Conclusions

The effect of Ta content on the solidification and microstructure characteristics of hot corrosion resistance Ni-based SX superalloys was investigated. The following conclusions are established.

(1) With increasing Ta content from 2wt% to 8wt%, the solidification temperature range increases from 39.0 to 61.8°C and the average primary dendrite arm spacing (PDAS) also increased because of the larger solidification temperature range.

(2) The segregation of refractory elements, especially Re and W, decreases with increasing Ta content. Ta addition excludes Re and W from the dendritic core to the interdendritic region.

(3) The size of γ′ precipitates in the dendrite core increases substantially from about 0.24 to 0.40 μm, whereas that of γ′ precipitates in the interdendritic region decreases slightly from 0.56 to 0.47 μm with increasing Ta content.

Acknowledgements

This work was supported by the National Natural Science Foundation of China (No. 51631008) and the National Key Research and Development Program of China (No. 2016YFB0701403).

References

[1] J.R. Nicholls, N.J. Simms, and A. Encinas-Oropesa, Modelling hot corrosion in industrial gas turbines, *Mater. High Temp.*, 24(2007), No. 3, p. 149.

[2] T.S. Sidhu, R.D. Agrawal, and S. Prakash, Hot corrosion of some superalloys and role of high-velocity oxy-fuel spray coatings—a review, *Surf. Coat. Technol.*, 198(2005), No. 1-3, p. 441.

[3] K. Matsugi, Y. Murata, M. Morinaga, and N. Yukawa, An electronic approach to alloy design and its application to Ni-based single-crystal superalloys, *Mater. Sci. Eng. A*, 172(1993), No. 1-2, p. 101.

[4] R.C. Reed, T. Tao, and N. Warnken, Alloys-By-Design: Application to nickel-based single crystal superalloys, *Acta Mater.*, 57(2009), No. 19, p. 5898.

[5] Z.X. Shi, J.R. Li, and S.Z. Liu, Effects of Ru on the microstructure and phase stability of a single crystal superalloy, *Int. J. Miner. Metall. Mater.*, 19(2012), No. 11, p. 1004.

[6] K. Matsugi, M. Kawakami, Y. Murata, M. Morinaga, and N. Yukawa, Accelerated oxidation of single crystal Ni–10Cr–12Al–Ta–W superalloys coated with a Na_2SO_4–NaCl salt, *Tetsu-to-Hagane*, 77(1991), No. 9, p. 1503.

[7] J.X. Chang, D. Wang, G. Zhang, L.H. Lou, and J. Zhang, Effect of Re and Ta on hot corrosion resistance of nickel-base single crystal superalloys, [in] M.C. Hardy, E.S. Huron, U. Glatzel, B. Griffin, B. Lewis, C. Rae, V. Seetharaman, and S. Tin, eds., *Superalloys 2016: Proceedings of the 13th Intenational Symposium on Superalloys*, Pennsylvania, 2016, p. 177.

[8] J.X. Chang, D. Wang, T. Liu, G. Zhang, L.H. Lou, and J. Zhang, Role of tantalum in the hot corrosion of a Ni-base single crystal superalloy, *Corros. Sci.*, 98(2015), p. 585.

[9] F.F. Han, J.X. Chang, H. Li, L.H. Lou, and J. Zhang, Influence of Ta content on hot corrosion behaviour of a directionally solidified nickel base superalloy, *J. Alloys Compd.*, 619(2015), p. 102.

[10] K.Y. Cheng, C.Y. Jo, T. Jin, and Z.Q. Hu, Effect of Re on the precipitation behavior of μ phase in several single crystal superalloys, *J. Alloys Compd.*, 536(2012), p. 7.

[11] T.M. Pollock and W.H. Murphy, The breakdown of single-crystal solidification in high refractory nickel-base alloys, *Metall. Mater. Trans. A*, 27(1996), No. 4, p. 1081.

[12] M.V. Nathal and L.J. Ebert, The influence of cobalt, tantalum, and tungsten on the microstructure of single crystal nickel-base superalloys, *Metall. Mater. Trans. A*, 16(1985), No. 10, p. 1849.

[13] L. Zheng, G. Zhang, T.L. Lee, M.J. Gorley, Y. Wang, C.B. Xiao, and Z. Li, The effects of Ta on the stress rupture properties and microstructural stability of a novel Ni-base superalloy for land-based high temperature applications, *Mater. Des.*, 61(2014), p. 61.

[14] J.S. Van Sluytman and T.M. Pollock, Optimal precipitate shapes in nickel-base γ–γ′ alloys, *Acta Mater.*, 60(2012), No. 4, p. 1771.

[15] C. Booth-Morrison, R.D. Noebe, and D.N. Seidman, Effects of tantalum on the temporal evolution of a model Ni–Al–Cr superalloy during phase decomposition, *Acta Mater.*, 57(2009), No. 3, p. 909.

[16] S. Gao, J.S. Hou, F. Yang, Y.G. Guo, C.S. Wang, and L.Z. Zhou, Effects of tantalum on microstructure and mechanical properties of cast IN617 alloy, *Mater. Sci. Eng. A*, 706 (2017), p. 153.

[17] S. Gao, J.S. Hou, F. Yang, Y.G. Guo, C.S. Wang, and L.Z. Zhou, Effect of Ta on microstructural evolution and mechanical properties of a solid-solution strengthening cast Ni-based alloy during long-term thermal exposure at 700°C, *J. Alloys Compd.*, 729(2017), p. 903.

[18] F.F. Han, *Effect of Al, Ti, Ta on Microstructure and Property of a Directionally Solidified Ni-base Superalloy* [Dissertation], University of Chinese Academy of Sciences, Shenyang, 2012, p. 61.

[19] Y.L. Tsai, S.F. Wang, H.Y. Bor, and Y.F. Hsu, Effects of alloy elements on microstructure and creep properties of fine-grained nickel-based superalloys at moderate temperatures, *Mater. Sci. Eng. A*, 571(2013), p. 155.

[20] Y.J. Sun and J. Zhang, Effects of Ta on microstructure and creep mechanism of a Ni-base single crystal superalloy, *Rare Met. Mater. Eng.*, 41(2012), No. 41, p. 1615.

[21] D.L. Sponseller, Differential thermal analysis of nickel-base superalloys, [in] *Superalloys 1996: Proceedings of the 8th International Symposium on Superalloys*, Pennsylvania, 1996, p. 259.

[22] Central Iron & Steel Research Institute; China Metallurgical information and Standardization Institute, GB/T 14999.7-2010: *Test Methods for Grain Sizes, Primary Dendrite Spacing and Microshrinkage of Superalloy Castings*, General Administration of Quality Supervision, Inspection and Quarantine of the People's Republic of China; Standardization Administration, 2010.

[23] Y.N. Yu and G.Q. Liu, *Stereology Organization: Principles and Applications of Quantitative Analysis*, Metallurgical Industry Press, Beijing, 1989.

[24] W. Kurz and D.J. Fisher, Dendrite growth at the limit of stability: tip radius and spacing, *Acta Metall.*, 29 (1981), p. 11.

[25] R. Gilles, D. Mukherji, H. Eckerlebe, L. Karge, P. Staron, P. Strunz, and T. Lippmann, Investigations of early stage precipitation in a tungsten-rich nickel-base superalloy using SAXS and SANS, *J. Alloys Compd.*, 612(2014), p. 90.

[26] J. Chen, J.K. Xiao, L.J. Zhang, and Y. Du, Interdiffusion in fcc Ni–X (X = Rh, Ta, W, Re and Ir) alloys, *J. Alloys Compd.*, 657(2016), p. 457.

[27] Y.Y. Qiu, Effect of the Al and Mo on the γ′/γ lattice mismatch and γ′ morphology in Ni-based superalloys, *Scr. Metall. Mater.*, 33(1995), p. 1961.

[28] P. Caron, High γ' solvus new generation nickel-based superalloys for single crystal turbine blade applications, [in] T.M. Pollock, R.D. Kissinger, R.R. Bowman, K.A. Green, M. McLean, S. Olson, and J.J. Schirra, eds, *Superalloys 2000: Proceedings of the 9th International Symposium on Superalloys*, Pennsylvania, 2000, p. 737.

[29] A.F. Giamei and D.L. Anton, Rhenium additions to a Ni-base superalloy: Effects on microstructure, *Metall. Trans. A*, 16(1985), No. 11, p. 1997.